Article

Optimised Design of An Arterial Network Model Reproduces Characteristic Central and Peripheral Hemodynamic Waveform Features in Young Adults

Avinash Kondiboyina[1,2], Hilary A. Harrington[1,3], Joseph J. Smolich[1,2], Michael M.H. Cheung[1,2,3] and Jonathan P Mynard[1,2,4,*]

[1] Heart Research, Murdoch Children's Research Institute, Parkville, VIC, Australia
[2] Department of Paediatrics, University of Melbourne, Parkville, VIC, Australia
[3] Department of Cardiology, Royal Children's Hospital, Parkville, VIC, Australia
[4] Department of Biomedical Engineering, University of Melbourne, Parkville, VIC, Australia
*Corresponding author: jonathan.mynard@mcri.edu.au

Key Points Summary:

- The origin of wave reflection in the arterial system is controversial, but reflection properties likely give rise to characteristic haemodynamics features in healthy young adults, including an early systolic peak, negative systolic augmentation, and diastolic hump in the ascending aortic pressure waveform, and triphasic flow in peripheral arteries. While computational modelling provides insights into arterial haemodynamics, no prior models have predicted all these features.
- An established arterial network model was optimised by incorporating 1) a more accurate representation of arterial wave speeds, 2) precisely matched junctions, and 3) impedance-preserving tapering, thus eliminating wave reflection in conduit arteries. Comparison with in vivo data (n=7) indicated that the characteristic waveform features in young adults were accurately predicted.
- Our findings strongly imply that a healthy young arterial system is structured to minimise wave reflection within the arterial network, and that wave reflection primarily occurs at microvascular beds.

Abstract The arterial network in healthy young adults is thought to be structured to minimise wave reflection in conduit arteries, producing an ascending aortic pressure waveform with three key features: early systolic peak, negative systolic augmentation, and diastolic hump. One-dimensional computer models have provided significant insights into arterial haemodynamics, but no previous models of the young adult have exhibited these three features. Since the latter was likely to be related to unrepresentative or non-optimised impedance properties of the model arterial networks, we developed a new 'YoungAdult' model that incorporated 1) a novel and more accurate empirical equation for approximating wave speeds, based on area and relative distance to elastic-muscular arterial transition points, 2) optimally-matched arterial junctions, and 3) an improved arterial network geometry that eliminated 'within-segment' taper (which causes wave reflection in conduit arteries) whilst establishing 'impedance-preserving' taper. These model properties led to wave reflection occurring predominantly at distal vascular beds, rather than in conduit arteries. The model predicted all three typical characteristics of an ascending aortic pressure waveform observed in young adults. When compared with non-invasively acquired pressure and velocity measurements (obtained via tonometry and Doppler ultrasound in 7 young adults), the model was also shown to reproduce the typical waveform morphology observed in the radial, brachial, carotid, temporal, femoral, and tibial arteries. The YoungAdult model provides support for the concept that the arterial tree impedance in healthy young adults is exquisitely optimised, and it provides an important baseline model for investigating cardiovascular changes in ageing and disease states.

Keywords: cardiovascular modelling; arterial haemodynamics; wave reflection

1. Introduction

It is widely recognised that a healthy arterial system limits the rise in pressure during systole and maintains pressure during diastole (O'Rourke, 1982; Nichols, 1998). It is thought that this occurs, in part, due to the "beautifully designed… tuning" of the arterial tree (O'Rourke & Hashimoto, 2007), resulting in reflected pressure waves predominantly arriving at the left ventricle during diastole. In the ascending aorta, this is evidenced by a Type C waveform, which has a similar shape to the flow waveform during systole—with an early systolic peak and negative augmentation index (AIx) (Kelly *et al.*, 1989)—and a pressure 'hump' during diastole that supports coronary perfusion (Murgo *et al.*, 1980; Nichols *et al.*, 1985; O'Rourke & Hashimoto, 2007). With ageing, arterial stiffening causes wave reflections to arrive during systole, which contributes to systolic hypertension, elevated left ventricular afterload and, ultimately, cardiovascular events and mortality (Lee & Oh, 2010; Chirinos *et al.*, 2012a; Chirinos *et al.*, 2012b; Tomiyama *et al.*, 2018; Sluyter *et al.*, 2019; Zhou *et al.*, 2021).

One-dimensional (1D) mathematical modelling of the arterial network is a powerful approach for gaining insight into the structural and functional properties that lead to this "beautiful tuning", as well as mechanisms underlying the detrimental effects of vascular ageing and disease (Stergiopulos *et al.*, 1992; Alastruey *et al.*, 2009; Charlton *et al.*, 2019). It therefore stands to reason that establishing a representative model of a healthy young adult is a crucial starting point for studying processes that might cause a departure from this 'ideal' arterial design. In particular, an accurate model of a young adult would be expected to exhibit the following characteristic features in the ascending aorta: 1) an early systolic peak, 2) a negative augmentation, and 3) a prominent diastolic hump. However, although the detailed model of Blanco *et al.* (2014) produced a diastolic hump, to our knowledge no prior models have predicted an early systolic peak and negative augmentation (Reymond *et al.*, 2012; Mynard & Smolich, 2015; Charlton *et al.*, 2019).

The reason(s) that these features have not been well-captured in existing 1D models is unclear, given that input variables such as wave speed in the ascending aorta (Groenink *et al.*, 1998; Rogers *et al.*, 2001; Kim *et al.*, 2013; Negoita *et al.*, 2018), and general haemodynamic variables e.g. systolic and diastolic blood pressures (Robinson & Brucer, 1939;

Master *et al.*, 1950; O'Rourke & Nichols, 2005) and cardiac output (Brandfonbrener *et al.*, 1955; Katori, 1979), have been representative of young adults. Nonetheless, at least four possible reasons may be involved in current 1D models not capturing all key features of young adult blood pressure waveforms. The first is that the wave speeds for the other arteries may not have been sufficiently representative of in vivo values. Since it is not feasible to obtain in vivo data from every artery in the body, previous investigators have estimated wave speeds of all arteries via an empirical equation that uses arterial diameter as the independent variable (Olufsen, 1999; Reymond *et al.*, 2009). However, since the common carotid and femoral arteries have comparable diameters—0.69 cm (Pomella *et al.*, 2017) and 0.77 cm (Lorbeer *et al.*, 2018), respectively—this approach leads to similar estimated wave speeds for both arteries. By contrast, in vivo measurements indicate that wave speed in the carotid artery—397–485 cm/s (Jourdan *et al.*, 2005; Petersen *et al.*, 2006; Rakobowchuk *et al.*, 2008; Engelen *et al.*, 2015; Mikola *et al.*, 2015)—is substantially lower than in the femoral artery—926–1029 cm/s (van den Berkmortel *et al.*, 1998; De Hoon *et al.*, 2003; Rakobowchuk *et al.*, 2009; Bossuyt *et al.*, 2015), most likely because the common carotid is an "elastic artery" (i.e. has a higher elastin content), whilst the femoral artery is a "muscular artery" (higher smooth muscle content) (Learoyd & Taylor, 1966; Lockwood *et al.*, 1992; Leloup *et al.*, 2015). As a rule of thumb, systemic arteries that are closer to the heart (e.g. aorta and carotid) are elastic while those further away (femoral and radial) are muscular (Betts *et al.*, 2013, p892-893). Thus, in this paper we propose a novel method for estimating the wave speed of all systemic arteries that accounts for the relative distance to transition points from elastic to muscular arteries.

A second possibility for the lack of young adult features in previous models is non-representative wave reflection properties of the arterial tree, given the profound influence of wave reflection on haemodynamic waveforms (van den Bos *et al.*, 1982). As previous models have exhibited positive systolic augmentation (Reymond *et al.*, 2012; Blanco *et al.*, 2014; Mynard & Smolich, 2015; Charlton *et al.*, 2019), wave reflection in these models likely occurred more proximally than is typical in young adults due to certain features of these geometrically simplified models. For example, similar to the related models by other authors (Westerhof *et al.*, 1969a; Avolio, 1980a; Stergiopulos *et al.*, 1992; Sherwin *et al.*, 2003; Reymond *et al.*, 2009; Blanco *et al.*, 2014), the model by Mynard and Smolich (2015) incorporated a substantial amount of taper in the brachial and femoral arteries (70% and 50% area reduction, respectively) and no side branches along their substantial length (35 and 44 cm, respectively). Such taper in the models is likely to produce substantial wave reflection (Segers & Verdonck, 2000); although the exact origin of wave reflection in the arterial system is controversial (Segers & Verdonck, 2000; Westerhof *et al.*, 2008), one widely-held theory is that wave reflection mainly occurs in the vicinity of resistance vessels (Hamilton, 1944; O'Rourke, 1984). If this is the case, it is likely that the progressive decline in diameter of conduit arteries with distance from the heart occurs primarily in a stepwise manner (decreasing where side branches arise), which allows for the preservation of impedance and minimises wave reflection. This stepwise reduction in diameter may therefore be considered "impedance-preserving taper" in contradistinction to "within-segment taper" that increases impedance and gives rise to wave reflection.

A third issue concerns the degree of wave reflection occurring at the distal vascular beds. In many previous models, the simulated velocity waveforms in peripheral arteries (such as the femoral artery) have been monophasic (forward flow throughout the cardiac cycle) (Stergiopulos *et al.*, 1992; Reymond *et al.*, 2009), whereas in vivo waveforms are triphasic (forward velocity during systole, reverse velocity during early diastole, and forward velocity again during late diastole) (Hwang, 2017; Kim *et al.*, 2020). It has been suggested that the early diastolic reverse flow arises due to the high resistance of peripheral vascular beds (Rittenhouse *et al.*, 1976; Maixner *et al.*, 1980), which in turn is likely to be associated with lower vascular bed compliance. Importantly, vascular bed compliance (not resistance per se) governs the reactive (or pulsatile) components of impedance, and hence the degree of wave reflection (Westerhof & Westerhof, 2018). However, while vascular bed compliance (C_{bed}) is therefore likely to be a key parameter governing systemic

arterial wave reflection, current methods for estimating C_{bed} for modelling studies are highly approximate. Thus, the in vivo value of C_{bed} is not known. In this paper, we therefore investigate the effect of C_{bed} on central and peripheral haemodynamics.

The fourth issue is that while most junctions in the systemic vasculature appear to be well-matched in the forward direction (Papageorgiou *et al.*, 1990), some studies suggest that the aorto-iliac bifurcation could be an exception to this rule, with a reflection coefficient (R_p) as high as 0.2 in some individuals (Greenwald *et al.*, 1990; Papageorgiou *et al.*, 1990). However, the effect of wave reflection at the aorto-iliac bifurcation on the wave reflection patterns in the aorta has not been explored in previous models.

This study had three main aims. The first was to determine the effect of incorporating the following improved physiological variables on large artery pressure and flow waveforms into a previously-described one-dimensional model by Mynard and Smolich (2015): a) a more accurate empirical equation that approximates arterial wave speeds based on cross-sectional area *and* relative distance to known elastic-muscular arterial transition points; and b) eliminating within-segment taper, and ensuring any taper in major arteries is impedance-preserving (e.g. by adding additional side branches). We hypothesized this improved 'YoungAdult' model would predict early systolic peak, negative augmentation, and diastolic hump in the ascending aortic pressure waveform, and triphasic flow in peripheral arteries. The second aim was to validate model predictions with non-invasively acquired in vivo pressure and velocity waveforms obtained from young adults, with a focus on whether the model reproduced key features of waveform morphology. The third aim was to determine the influence of the following key aspects of the model: a) compliance of distal vascular beds (C_{bed}), b) reflection coefficient of the aorto-iliac bifurcation, and c) employing impedance-preserving vs within-segment arterial taper on arterial wave reflection.

2. Methods

2.1. Wave Speed Relationship - Conventional Approach

Previous modelling studies defined the relationship between arterial diameter and wave speed by fitting exponential (Olufsen, 1999) or power (Reymond *et al.*, 2009) curves to in vivo data. In doing so, the elastic/muscular nature of arteries has not been explicitly accounted for. To evaluate this approach, in vivo data on the wave speeds of various arteries in young adults (18-30 years) were gathered from literature, the details of which are presented in Supplemental File 1 – Part A. Similar to previous work, a power relationship (Equation 1) was fitted to the data points using the Curve Fitting toolbox of MATLAB (Mathworks, Massachusetts, USA). Furthermore, we imposed an anchor point for the fitted curve at the wave speed of the ascending aorta (Segment 2), as we considered this to be the most important value for achieving representative arterial compliance. To achieve this, a weight of 1 was given to the wave speeds of all other arteries, while the weight of the ascending aortic wave speed was arbitrarily increased to a value (50) that forced the curve to pass exactly through this wave speed. This manipulation did not significantly alter the shape of the curve compared to using no weights (data not shown). The resulting power law equation was:

$$c = \frac{577.3}{A^{0.23}} \qquad \text{(Equation 1)}$$

where c is wave speed (cm/s) and A is artery area (cm^2). This relationship yielded an R^2 value of 0.79 and a root mean square error (RMSE) of 177 cm/s (Figure 1a). However, there were substantial differences between the in vivo wave speeds and those calculated using this equation (Figure 1b). For example, the in vivo wave speeds of the carotid and femoral arteries were 438 cm/s and 905 cm/s (average of literature values – refer to Supplemental File 1), respectively, whereas Equation (1) yielded 679 cm/s (difference = -241 cm/s) and 703 cm/s (difference = 202 cm/s), respectively.

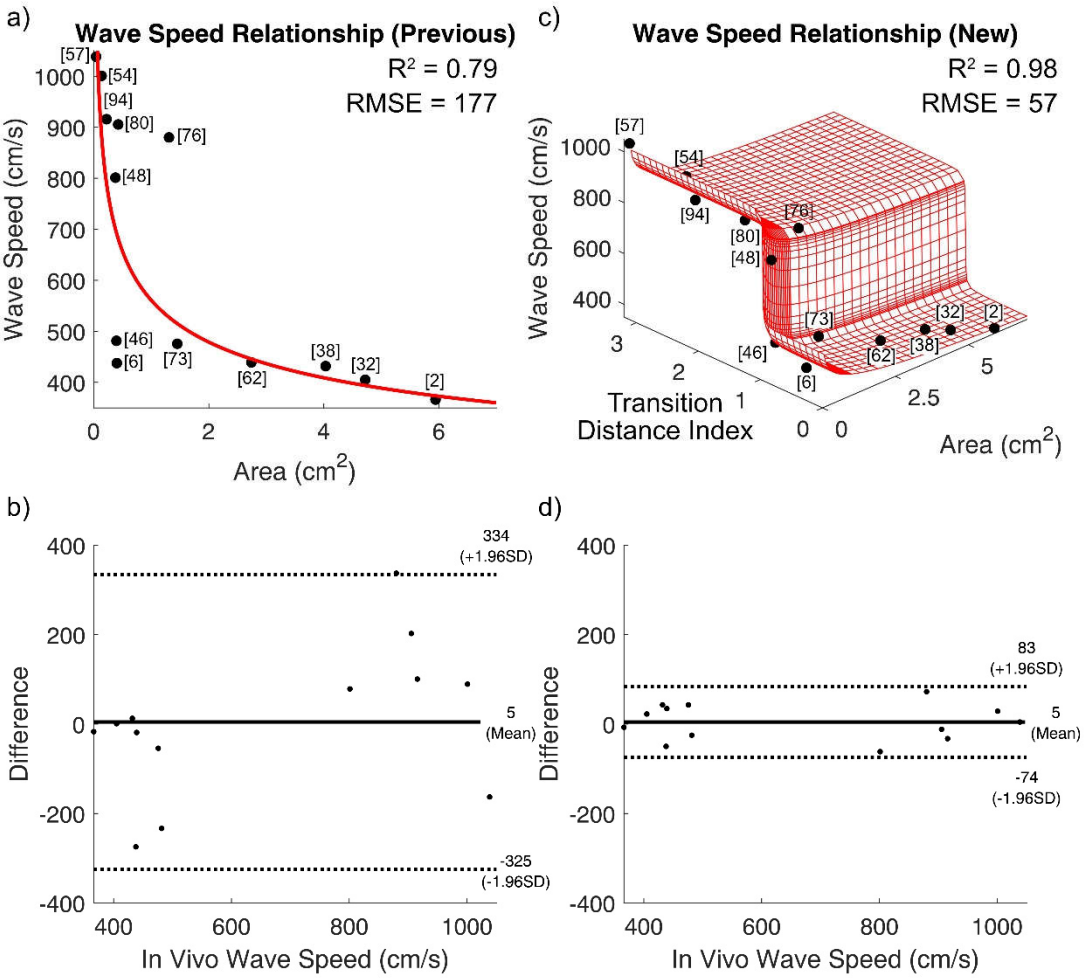

Figure 1. Wave speed estimated only from artery area as in previous studies (a), and that estimated from the artery area and transition distance index in this study (b). The numbers in square brackets correspond to the segment number of the artery (see Figure 2). Bland Altman plots depict the difference between in vivo wave speeds and those calculated using the previous and new relationships are show in (b) and (d), respectively.

2.2. Wave Speed Relationship - Accounting for elastic-muscular transition points

In addition to elastic arteries being closer to the heart and muscular arteries being further away, there are known transition points along a given arterial pathway where there is a substantial increase in wave speed and distinct change in morphological features from one artery to the next; this indicates a transition from a predominantly elastic to more muscular arteries. These points are the distal ends of the axillary artery for the upper limbs (Bjarnegård & Länne, 2010) and abdominal aorta for the lower limbs (Latham *et al.*, 1985), and 1 cm from the origin of the external carotid artery for the head and neck region (Nowrozani & Zareiyan, 2011) (we here assume the same distance for internal carotid artery, consistent with its classification as a muscular artery (Rees, 1968)). Using this, we propose a "transition distance index" (TDI) of an artery as a surrogate marker for an artery's degree of elasticity/muscularity. TDI is defined as the distance between the proximal end of an artery and the left ventricle divided by the distance between the transition point and the left ventricle. Thus, TDI < 1 and TDI > 1 indicates an elastic and muscular artery, respectively.

The transition points at the axillary artery, abdominal aorta, and external carotid artery were assigned to the arm arteries (subclavian to ulnar and radial arteries), the entire aorta and leg arteries (ascending aorta to posterior tibial artery), and the cerebral arteries

(all arteries distal to the common carotid and vertebral arteries inclusive), respectively. The TDI of arteries with available in vivo data on wave speed and area are shown in Supplemental File 1 – Part A. Power and sigmoid functions were used to govern the area- and TDI-dependence of wave speed, respectively. Thus, a 3D surface was obtained with area and TDI as independent variables and wave speed as the dependent variable (Equation 2). After weighting towards the ascending aortic data point in the same way as for Eq (1), the final expression was:

$$c = \frac{661}{A^{0.058}} + 145.3 \times \arctan\left(167 \times TDI - 164.8\right) \qquad \text{(Equation 2)}$$

This relationship yielded an R^2 value of 0.98 and RMSE of 57 cm/s (Figure 1c). The differences between the in vivo wave speeds and those calculated using the new relationship were substantially reduced compared to those obtained with Equation (1) (Figure 1d), with values of 462 cm/s and 921 cm/s for the carotid and femoral arteries (differences of only -24 cm/s and -15 cm/s from the in vivo values, respectively, see Supplemental File 1).

2.3. Model Development

The YoungAdult 1D model described herein is an adaptation of a previously developed closed-loop model of the entire circulation and 4-chamber heart, herein referred to as 'Mynard2015' (Mynard & Smolich, 2015). Since the present study only relates to systemic arterial haemodynamics, only those model components likely to have a substantial impact on large artery haemodynamics were incorporated; therefore the coronary arteries, veins and the pulmonary circulation were removed, whereas the cerebral arteries were retained, as these have been shown to have an effect on central waveforms (Reymond *et al.*, 2009). The input to the YoungAdult model was a 2-chamber elastance-based heart model (left atrium and ventricle) that has been described previously (Kondiboyina *et al.*, 2020). The distal arteries were terminated with lumped parameter 3-element windkessel compartments representing downstream vascular beds.

Eliminating the veins, pulmonary and coronary circulations, and inter-ventricular interactions caused small changes in the preload, mean arterial pressure, and chamber elastance, respectively, compared with the closed-loop model. To achieve results that were similar to those of the Mynard2015 model, we used an algorithm to iteratively adjust the preload, vascular resistance, and chamber elastance until the maximum chamber volume, mean aortic pressure, and maximum effective chamber elastance, respectively, of the YoungAdult model were within a 0.5% tolerance of those of the Mynard2015 model. Final parameters for the heart model and vascular resistances are provided in Supplemental File 1 - Part B.

2.3.1. Tapering and Arterial Side Branches

To obtain impedance-preserving taper and reduce early wave reflection, side branches were added to the major arterial segments of the YoungAdult model—such as the internal carotid, radial, brachial, and femoral arteries. The brachial artery, which originally had a 71% area taper, was divided into 4 non-tapered segments of successively smaller diameter by adding side branches along its length based on the detailed model of Blanco *et al.* (2014). Similarly, the femoral artery, which originally had an area taper of 43%, was divided into 5 non-tapered segments of successively smaller diameter by adding 4 equally spaced side branches representing the muscular branches of the femoral artery that perfuse the surrounding tissue. Furthermore, a more detailed lower limb arterial network was included in the model by including the genicular, popliteal and peroneal arteries, which have been neglected in most previous models. Figure 2 depicts a schematic representation of the model and the detailed list of all arteries included in the YoungAdult model can be found in Supplemental File 2.

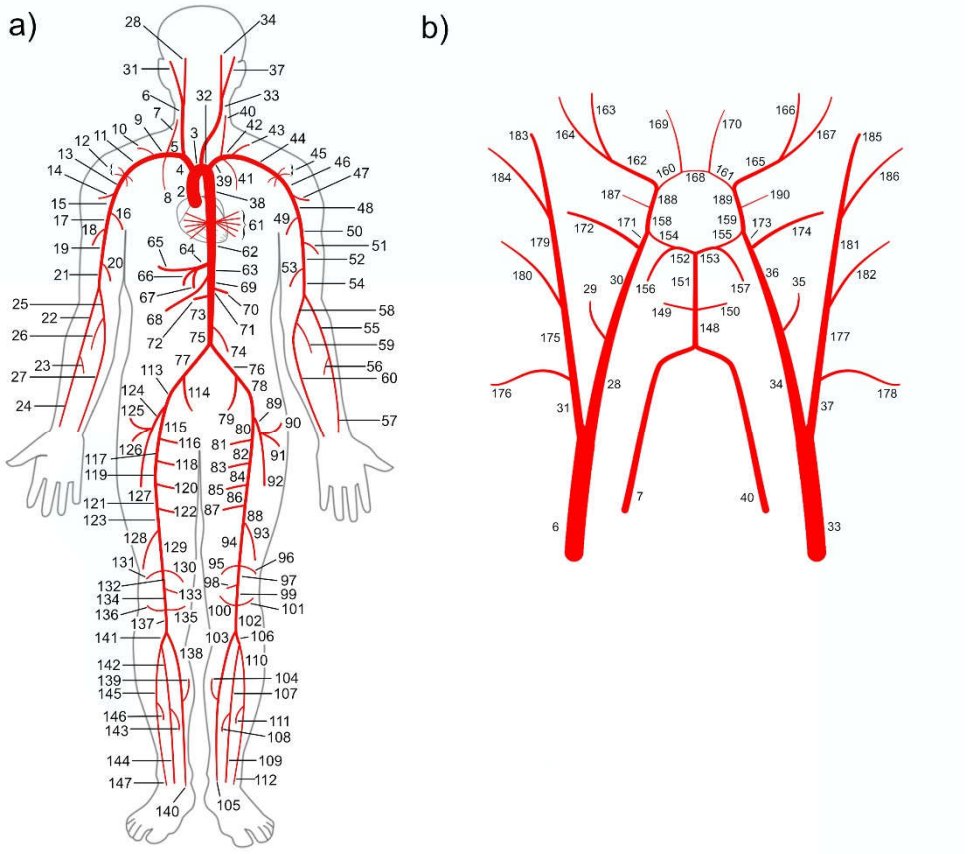

Figure 2. Schematic diagram of the systemic (a) and cerebral (b) arteries of the YoungAdult model.

2.3.2. Impedance Matching of Branch Junctions

Arterial junctions have been found to be relatively well-matched (i.e. R_p of approximately zero) in vivo, implying an efficient transmission of energy in the forward direction (Papageorgiou *et al.*, 1990). However, simply eliminating within-segment taper from arteries of the YoungAdult model would result in unmatched junctions. We therefore developed an optimization algorithm to produce well-matched junctions for all arteries in the YoungAdult model. The R_p value at a junction can be calculated using Equation 3.

$$R_p = \frac{\frac{A_0}{c_0} - \frac{A_1}{c_1} - \frac{A_2}{c_2}}{\frac{A_0}{c_0} + \frac{A_1}{c_1} + \frac{A_2}{c_2}} \qquad \text{(Equation 3)}$$

where the subscript '0' refers to the parent artery while '1' and '2' refers to the two daughter arteries. As part of the optimization algorithm (Eq 3), the area and wave speed of the parent artery was kept fixed, while A_1 and A_2 were multiplied by an unknown factor (x); the corresponding wave speeds (c_1 and c_2) were calculated using Equation 2. Using the fminsearch function of MATLAB (Mathworks, Massachusetts, USA), the value of x was iteratively changed until a reflection coefficient of 0 was achieved (within a tolerance of ± 0.001). The optimization algorithm did not significantly alter the diameters of the downstream arteries, as evidenced by the terminal posterior tibial (Black *et al.*, 2003; Sabatier *et al.*, 2006) and radial arteries (Yoo *et al.*, 2003; Yoo *et al.*, 2005; Beniwal *et al.*, 2014), which had diameters within physiological ranges. Note that the within-segment taper of the cerebral arteries downstream of the internal carotid artery from the Mynard2015 model was retained because the looping nature of the cerebral arterial tree meant that some cerebral arteries had two parents. This is not conducive for the optimization algorithm, which requires a simple bifurcating tree structure.

To explore the influence of reflection at the aorto-iliac bifurcation, the optimization algorithm was used to obtain a second model in which a R_p value of 0.2 was enforced at

the aorto-iliac bifurcation, along with well-matched junctions in the downstream junctions of the legs.

2.3.3. Vascular Bed Compliance

The compliance of distal vascular beds (C_{bed}) is difficult to measure in vivo and estimation techniques are therefore used for model parameterisation. In most studies, total arterial compliance (TAC_{wk}) has first been estimated from aortic pressure and flow waveforms via the pulse pressure method that uses a 2-element windkessel model (Stergiopulos *et al.*, 1994). Vascular bed compliance is then estimated by subtracting the combined compliance of all 1D arterial segments from TAC_{wk} and distributing the remaining compliance among the vascular beds (in inverse proportion to their resistances). While the windkessel method is well established to estimate arterial compliance, it is not known whether this 'subtraction approach' accurately captures both central arterial compliance (C_{art}) and C_{bed}.

In Supplemental File 1 – Part C, we show that although TAC_{wk} is sensitive to C_{art}, it is relatively insensitive to C_{bed} in the YoungAdult model, with an increase in TAC_m by 153% leading to only a 1.6% increase in TAC_{wk}. This suggests that currently used methods of estimating C_{bed} may be inaccurate. We thus investigated the effect of varying C_{bed} on the model waveforms. C_{bed} and R_{bed} (windkessel resistance) are related via an assumed time constant ($\tau = R_{bed} \times C_{bed}$). Starting from a value of $\tau = 0.55$, as used in Mynard2015, we found that a value of $\tau = 1.3$ produced the characteristic features of a young adult aortic pressure waveform (early systolic peak, diastolic hump, and negative augmentation) and in the peripheral flow waveforms (triphasic flow). Thus, C_{bed} of all vascular beds was calculated using R_{bed} and $\tau = 1.3$ as the baseline model. The details of the vascular beds of the YoungAdult model with baseline C_{bed} values can be found in Supplemental File 3. The sensitivity of the model to the value of τ was also tested by performing simulations with $\tau = 0.5$ and $\tau = 2.5$.

2.3.4. Impact of Impedance-Preserving vs Within-Segment Taper

To elucidate the impact of employing impedance-preserving taper on central wave reflection, the closed-loop Mynard2015 model (with a substantial degree of within-segment taper) was first converted to an open-loop model, as described above, but without any other changes to the arterial tree geometry or wave speed. The C_{bed} of all vascular beds was then calculated based on R_{bed} and a value of τ of 1.3 (baseline) and 100 (used to markedly reduce wave reflection at vascular beds and thereby reveal the contribution of tapering to wave reflection). The same procedure was followed for the YoungAdult model, which has no within-segment taper (i.e. only impedance-preserving taper), except in the cerebral arteries. The waveforms at the aorta of the two models were then compared for both values of τ.

To quantify the effects of taper on central wave reflection, we calculated the system 'input pressure' (P_{in}, elsewhere called the water hammer pressure (Vennin *et al.*, 2021), which signifies the pressure that would occur in the absence of any wave reflection) as $P_{in} = QZ_c$ (Phan *et al.*, 2016), where Q is flow and Z_c is characteristic impedance calculated using the frequency-domain method (O'Rourke & Taylor, 1967). Conversely, the 'total reflected pressure' (P_{ref}), defined as the pressure arising from vascular wave reflection and any re-reflections occurring at the ventricle, is given by $P_{ref} = P - P_{in} = 2P_{bk}$, where P is the total pressure and P_{bk} is the traditionally defined backward component of pressure obtained by wave separation (Westerhof *et al.*, 1972). In summary, $P = P_{in} + P_{ref}$ and as wave reflection decreases, $P_{ref} \to 0$ and $P \to P_{in}$ (Phan *et al.*, 2016).

2.3.5. Model Computation

The model was implemented using previously described methods (Mynard & Nithiarasu, 2008; Mynard & Smolich, 2015). In brief, the non-linear 1D form of the Navier-Stokes equations, combined with a non-linear viscoelastic pressure-area relationship

(Mynard & Smolich, 2015), were solved using a finite element method (Mynard & Nithiarasu, 2008), with conservation of mass and continuity of total pressure enforced at junctions.

2.4. Model Validation with In Vivo Data

2.4.1. Non-Invasive Study

Model-predicted pressure and velocity waveforms were validated by performing applanation tonometry and Doppler ultrasound measurements, respectively, of accessible arteries in 7 healthy young adults aged between 21 and 25 years. Informed consent was obtained from all participants and the study conformed to the standards set by the Declaration of Helsinki. The study was approved by the Ethics Committee of the Royal Children's Hospital, Victoria, Australia. Participants were asked to refrain from consuming caffeine or alcohol for 3 hours prior to the study and all participants were non-smokers. They were placed in a supine position and were allowed to rest for 5 minutes before recording their brachial blood pressure with an oscillometric device (WatchBP Office Central, Microlife, Switzerland). Pressure waveforms in the left brachial, radial, common carotid, superficial femoral, superficial temporal, and posterior tibial arteries were then measured with applanation tonometry (SPT-301, Millar Instruments, Texas, USA). The pressure waveform of the ascending aorta was obtained by applying a validated transfer function to the common carotid pressure waveform (Chen *et al.*, 1996). Finally, Doppler ultrasound was performed using a GE Vivid ultrasound machine (10-15 MHz; GE Healthcare, NSW, Australia) for the left common carotid and femoral arteries and a VisualSonics Vevo 3100 ultrasound machine (30-70 MHz; FUJIFILM VisualSonics, Toronto, Canada) for the left brachial, radial, and posterior tibial arteries owing to the difference in depth of the arteries. The sampling gate was over the middle two-thirds of the artery with an insonation angle of less than 60^0 (Gerhard-Herman *et al.*, 2006). Doppler ultrasound of the superficial temporal artery was not performed.

2.4.2. In Vivo Data Analysis

Pressure waveforms from tonometry were ensemble-averaged over approximately 20 heart beats. Systolic and pulse pressures for each artery were obtained by calibrating waveforms to diastolic and mean brachial pressures, since these pressures are similar throughout the arterial network (Hansen & Orskov, 1992; Kelly & Fitchett, 1992). The upper and lower spectral envelopes of the Doppler ultrasound data were automatically segmented using a custom program written in MATLAB 2019b (R2020b, The MathWorks Inc., Natick, Massachusetts). In each artery, the mean velocity waveform across 3 cycles was calculated from the spectrum-weighted average, which were then ensemble averaged.

To facilitate visual comparison of in vivo and model waveforms, pressure, and velocity waveforms were normalized to an amplitude of 1. To normalize the systolic duration, pressure waveforms with a distinct dicrotic notch (common carotid, superficial temporal, and ascending aortic waveforms) were normalized to a systolic duration of 0.3 s (the same as that of the model). The waveforms in other arteries did not always have a sharply defined dicrotic notch indicating the end of systole, and so these waveforms were scaled horizontally to minimise the root mean squared error compared with the corresponding model waveform. These were then ensemble-averaged to visually validate the corresponding waveforms produced by the model. Validation of raw absolute values of pressure and velocity (systolic and pulse) are also tabulated.

3. Results

3.1. Comparison With Previous Models

Figure 3 compares the aortic pressure waveforms from the YoungAdult model with those from previous models. The YoungAdult model displayed all features typically found in young adults: early systolic peak (at 35% of systolic duration), negative augmentation (AIx = -3.6%), and a clear diastolic hump. By comparison, previous models

exhibited later systolic peaks (between 53% and 75% of systolic duration) and positive augmentation (AIx between 3.4%, and 24%), while only the Blanco model displayed a diastolic hump.

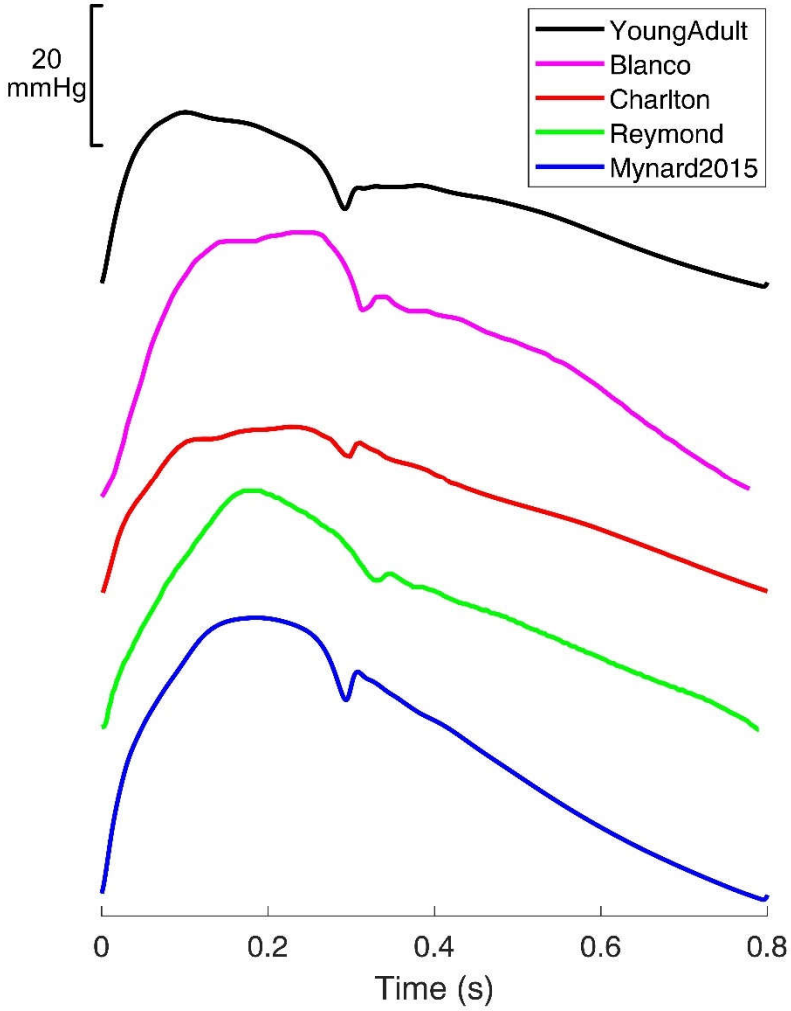

Figure 3. Comparison of the ascending aortic pressure waveform of the YoungAdult model with models described by Blanco et al (Blanco *et al.*, 2014), Charlton et al (Charlton *et al.*, 2019), Reymond et al (Reymond *et al.*, 2012), and Mynard et al (Mynard2015) (Mynard & Smolich, 2015).

3.2. In Vivo Validation

Participant characteristics are presented in Table 1 and their pressure and flow waveforms are presented in the top panels of Figures 4-6. There are no pressure scales in these figures because our primary aim was to visually compare the model waveforms with in vivo ones. Overall, pressure and velocity waveforms produced by the baseline YoungAdult model ($\tau = 1.3$) were similar to those found in vivo. Importantly, the model captured key features of young adult waveforms such as triphasic flow in distal arteries (brachial, radial, femoral, and tibial) and an aortic pressure waveform that matched the in vivo waveform. Furthermore, Table 2 shows that the systolic and pulse pressures, and maximum and pulse velocity values of all arteries of the model were within the range of values found in vivo, with the exception of ascending aortic pulse pressure (although the model values were similar to the central pulse pressure reported in 18-29-year-olds in a much larger study (McEniery *et al.*, 2005)).

Table 1. Characteristics of participants in the in vivo validation study (n = 7).

Age (years)	22.6 ± 1.5
Height (cm)	172.2 ± 7.8
Weight (kg)	64.4 ± 15.7
Sex (% Male)	29%

Table 2. Comparison of the systolic/maximum and pulse pressure and velocity values as median (range) across various arteries from the YoungAdult model and the in vivo study (subject characteristics given in Table 1).

Artery	Pressure/Velocity	Units	Model Values	In Vivo Values
Ascending Aorta	Pressure (Systolic)	mmHg	105	102 (96 – 122)
	Pressure (Pulse)	mmHg	25	35 (33 – 52)
Left Common Carotid Artery	Pressure (Systolic)	mmHg	111	102 (95 – 120)
	Pressure (Pulse)	mmHg	32	37 (31 – 50)
	Velocity (Max)	cm/s	54	44 (38 – 89)
	Velocity (Pulse)	cm/s	52	36 (30 – 69)
Left Brachial Artery	Pressure (Systolic)	mmHg	117	112 (105 – 126)
	Pressure (Pulse)	mmHg	39	41 (34 – 56)
	Velocity (Max)	cm/s	35	49 (26 – 64)
	Velocity (Pulse)	cm/s	40	57 (34 – 79)
Left Radial Artery	Pressure (Systolic)	mmHg	113	116 (114 – 145)
	Pressure (Pulse)	mmHg	36	49 (45 – 75)
	Velocity (Max)	cm/s	30	20 (15 – 39)
	Velocity (Pulse)	cm/s	33	29 (21 – 43)
Left Superficial Femoral Artery	Pressure (Systolic)	mmHg	122	106 (98 – 127)
	Pressure (Pulse)	mmHg	45	41 (30 – 57)
	Velocity (Max)	cm/s	36	37 (32 – 68)
	Velocity (Pulse)	cm/s	42	48 (32 – 89)
Left Posterior Tibial Artery	Pressure (Systolic)	mmHg	118	124 (114 – 134)
	Pressure (Pulse)	mmHg	43	52 (43 – 68)
	Velocity (Max)	cm/s	36	21 (13 – 43)
	Velocity (Pulse)	cm/s	40	31 (18 – 59)
Left Superficial Temporal Artery	Pressure (Systolic)	mmHg	113	105 (94 – 129)
	Pressure (Pulse)	mmHg	35	36 (30 – 59)

3.3. Influence of Vascular Bed Compliance

Decreasing the compliance of the arm vascular beds by decreasing τ increased the triphasic nature of the flow waveforms of the brachial and radial arteries, with increasing amplitudes of the systolic forward flow, early diastolic reverse flow and late diastolic forward flow, and earlier diastolic flow reversal. Similar changes were also observed in the pressure waveforms, with an increased systolic peak, lower early diastolic trough, and a higher late diastolic peak. This also augmented the late systolic portion of the ascending aortic pressure waveform. Increasing compliance had the opposite effect, with decreasing flow and pressure amplitudes and reduced late systolic augmentation (Figure 4).

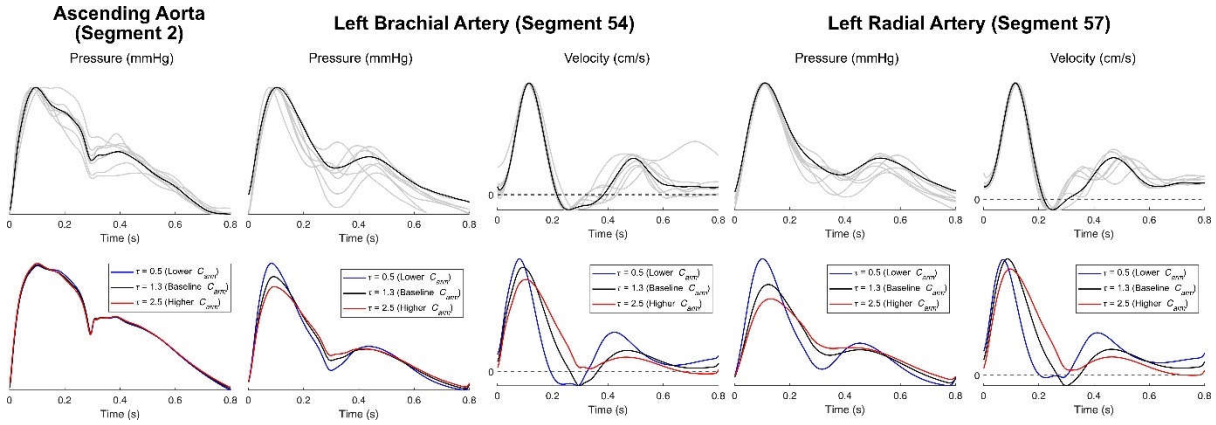

Figure 4. Comparison of the ascending aortic, left brachial, and left radial artery waveforms produced by the YoungAdult model and in vivo data. The effect of varying the compliance of the arm vascular beds (C_{arm}) by varying the time constant (τ) on the waveforms is also shown. The in vivo waveforms have been normalized for visualization purposes.

A similar effect was seen when decreasing and increasing leg vascular bed compliance (Figure 5). Importantly, decreasing compliance augmented the diastolic hump of the ascending aortic pressure waveform, while increasing compliance had the opposite effect.

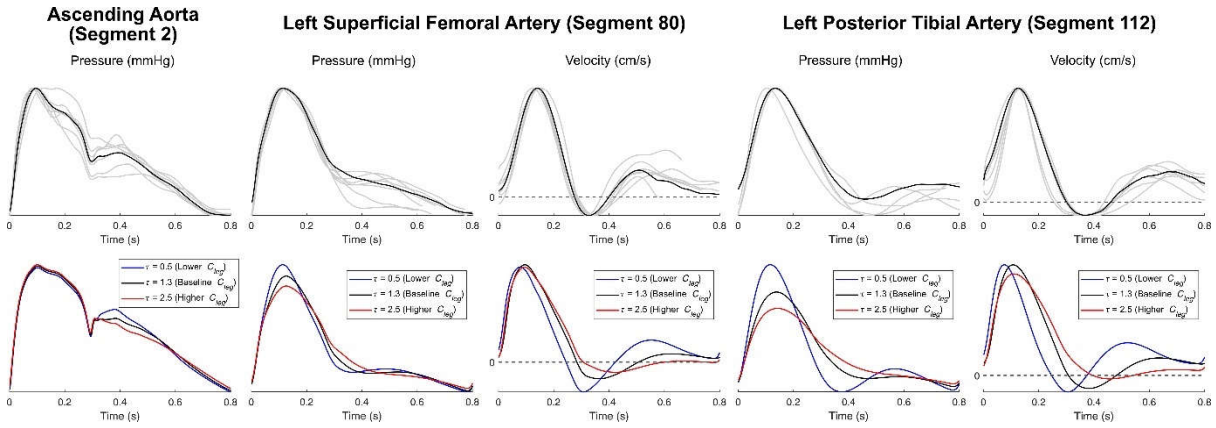

Figure 5. Comparison of the ascending aortic, left superficial femoral, and left posterior tibial artery waveforms produced by the YoungAdult model and in vivo data. The effect of varying the compliance of the leg vascular beds (C_{leg}) by varying the time constant (τ) on the waveforms is also shown. The in vivo waveforms have been normalized for visualization purposes.

Increasing the cerebral vascular bed compliance also caused similar changes in the pressure waveforms of the common carotid and superficial temporal arteries, and slightly augmented the late systolic portion of the ascending aortic pressure waveform (Figure 6).

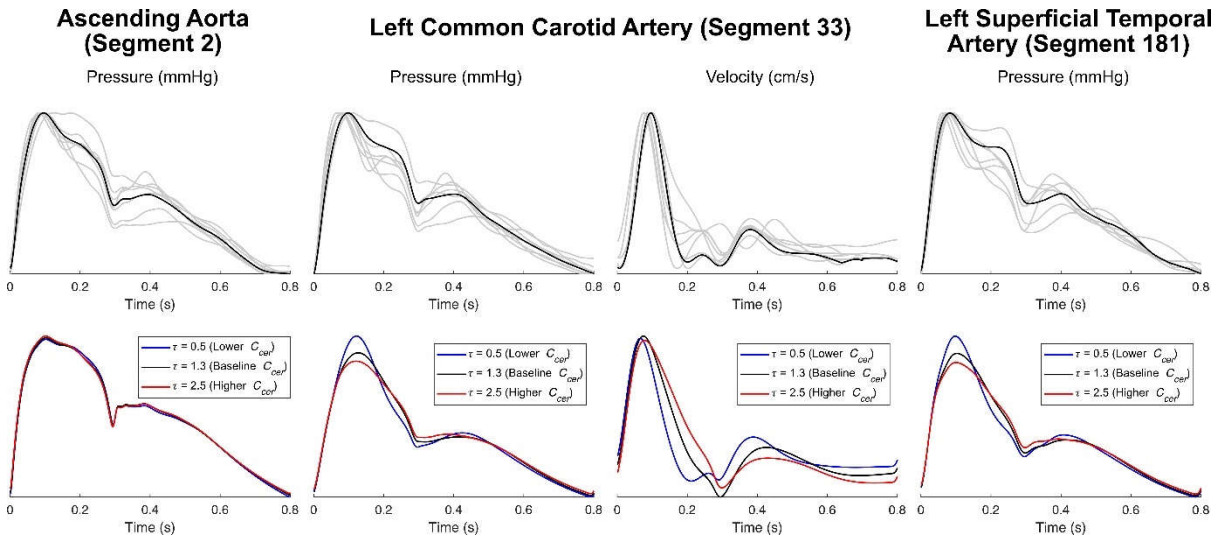

Figure 6. Comparison of the ascending aortic, left common carotid, and left superficial temporal artery waveforms produced by the YoungAdult model and in vivo data. The effect of varying the compliance of the cerebral vascular beds (C_{cer}) by varying the time constant (τ) on the waveforms is also shown. The in vivo waveforms have been normalized for visualization purposes. The velocity profile of the superficial temporal artery was not measured.

3.4. Wave Reflection at the Aortoiliac Bifurcation

Introducing a reflection coefficient of 0.2 at the aortoiliac bifurcation and adjusting the downstream leg vasculature to maintain well-matched junctions thereafter affected the late systolic and diastolic portions of the ascending aortic pressure waveform and abolished the diastolic hump. It also increased the height of the dicrotic notch (Figure 7a) and masked the effect of changing leg vascular bed compliance on the ascending aortic pressure waveform, with decreasing compliance causing lesser modulation of the diastolic hump (Figure 7b) when compared to the changes seen in Figure 5 (where $R_p = 0$).

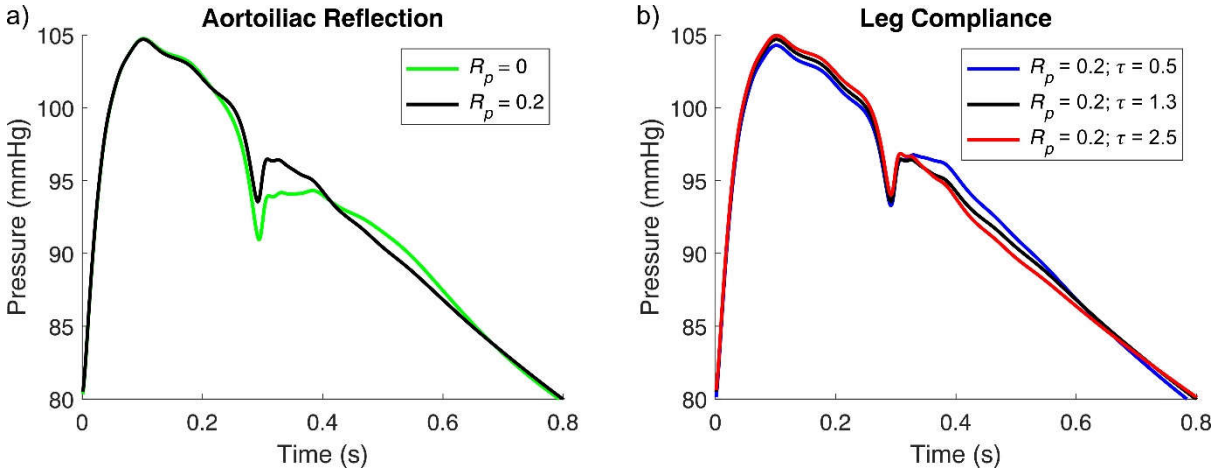

Figure 7. a) Comparison of the ascending aortic pressure waveform of the YoungAdult model with an aortoiliac bifurcation reflection coefficient of 0 (baseline) and 0.2. b) Effect of changing leg vascular bed compliance on the ascending aortic pressure waveform when aortoiliac R = 0.2.

3.5. Impact of Tapering on Wave Reflection

To investigate the impact of impedance-preserving vs within-segment tapering on arterial wave reflection, Figure 8 shows the effect of a large increase in C_{bed} that markedly reduced wave reflection in the distal vascular beds (thus revealing the contribution of wave reflection within the 1D network). In the Mynard2015 model (which includes substantial within-segment taper), the amplitude of P_{ref} at the aorta was 29 mmHg at

baseline and reduced by only 27% when C_{bed} was increased; there also remained a large difference between P (blue) and P_{in} (green, Figure 8b). On the other hand, the amplitude of P_{ref} in the ascending aorta of the YoungAdult model (with mostly impedance-preserving taper) was 17 mmHg at baseline (43% less than the Mynard2015 model) and reduced by 63% with increased C_{bed}; the ascending aortic pressure and input waveforms also became very similar in shape (Figure 8d), demonstrating that most of the wave reflection in the YoungAdult model arises at the level of the vascular beds.

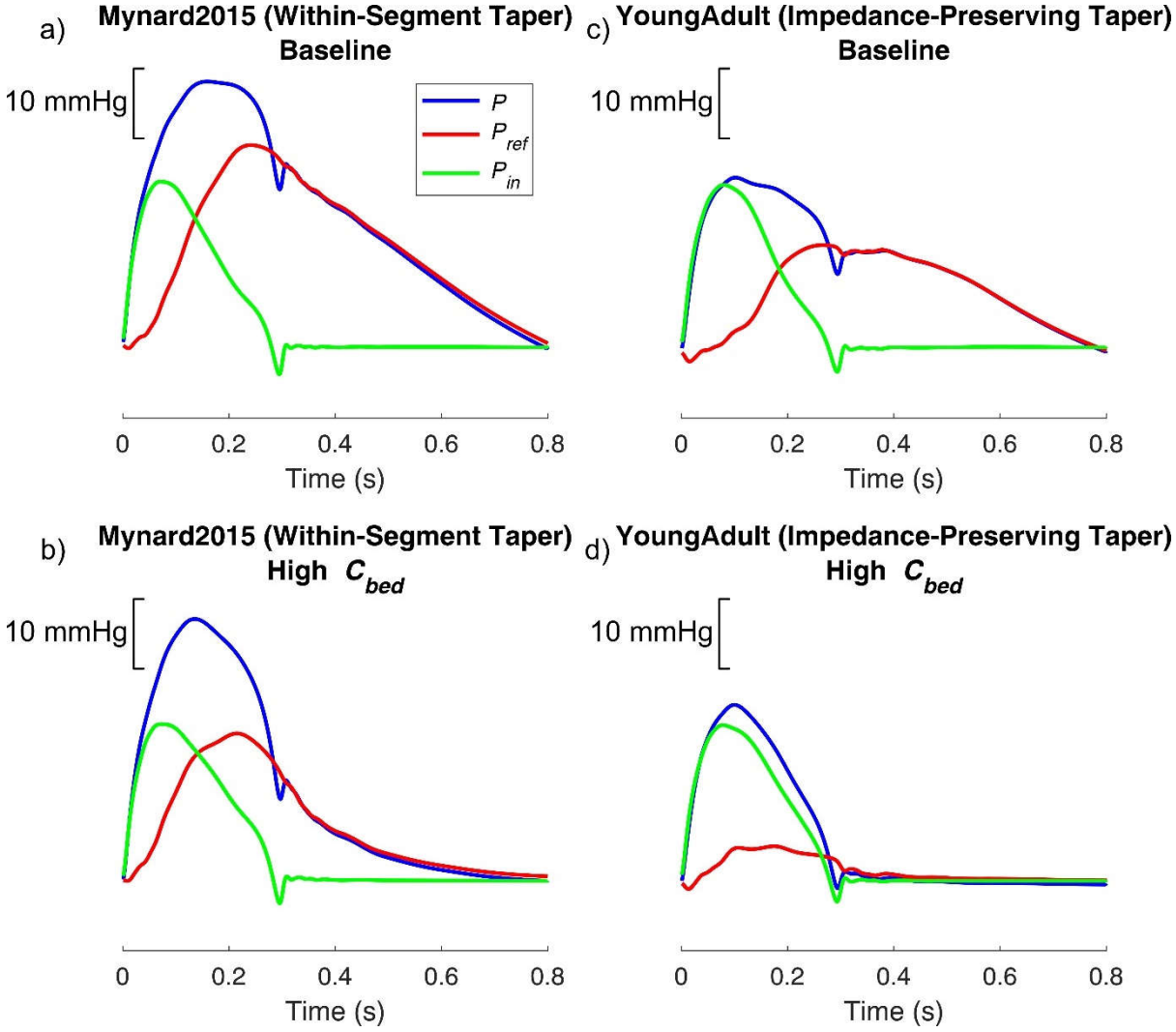

Figure 8. Comparing the effect of arterial taper on wave reflection. The Mynard2015 incorporated substantial within-segment taper (as in most other models), whereas the YoungAdult model eliminated within-segment taper by adding impedance-preserving side branches. The total pressure (P), input pressure (P_{in}), and total reflected pressure (P_{ref}) waveforms of the aorta are shown for the Mynard2015 and YoungAdult models with baseline vascular bed compliance (C_{bed}) (a and c, respectively) and, to evaluate the influence of substantially reducing wave reflection from all distal vascular beds via a 100-fold increase in C_{bed} (b and d, respectively). The ascending aortic pressure waveform has been shifted to start at zero for better visual comparison with the input and reflected pressure waveforms.

4. Discussion

This study described an optimised arterial network model that is the first to predict the characteristic features of the ascending aortic pressure waveform in young adults (early systolic peak, negative augmentation, and a diastolic hump (Murgo *et al.*, 1980; Nichols *et al.*, 1985; O'Rourke & Hashimoto, 2007)) as well as clearly triphasic velocity profiles in peripheral arteries. The properties of the YoungAdult model that led to this

improvement over prior models were: 1) an improved wave speed relationship that accounted for the degree of elasticity/muscularity of arteries in addition to area, 2) optimally matched junctions, 3) impedance-preserving taper and 4) increased vascular bed compliance. Model results imply that the arterial network must be exquisitely well-matched to exhibit the observed waveform features that are typical of healthy young adults, with minimal reflection in the main conduit arteries (i.e. at junctions or due to within-segment taper), and wave reflection predominantly occurring in the distal vascular beds. Furthermore, a major strength of our study is that both pressure and velocity waveforms produced by the model across major central and peripheral arteries were in close agreement with observed in vivo data measured in young adults.

We have proposed a novel empirical equation that uses both area and distance from the heart indexed to known transition points as a surrogate marker of the degree of elasticity/muscularity. Owing to the paucity of data on the wave speed of every artery, prior studies have employed different estimation techniques for the purpose of model parameterisation. Westerhof *et al.* (1969b) assigned an elastic modulus (E) to each artery and then calculated wave speed using the Moens-Korteweg equation: $c = \sqrt{Eh/2r\rho}$, where ρ is blood density, and h and r are wall thickness and artery radius, respectively, using data from Noordergraaf *et al.* (1963). Although the value of E increased in a stepwise manner (4, 8, and 16 $\times$ 10^6 g cm^{-1} s^{-2}) with increasing distance along an arterial path (Westerhof *et al.*, 1969b), the common carotid and femoral arteries were both assigned the same value of E (4 $\times$ 10^6 g cm^{-1} s^{-2}) and thus had similar wave speeds (582 cm/s and 625 cm/s, respectively). This approach was also employed by Stergiopulos *et al.* (1992) and Avolio (1980b), although Avolio increased the value of E for the femoral artery to 8 $\times$ 10^6 g cm^{-1} s^{-2}, which increased its wave speed to 910 cm/s and was therefore more representative of in vivo values.

To avoid the need to estimate E and h for every artery, Olufsen (1999) used data from Westerhof *et al.* (1969b) and Stergiopulos *et al.* (1992) to develop an empirical relationship between Eh/r and r. This allows the estimation of the wave speed of an artery based solely on its radius. This relationship has been employed in multiple studies (Mynard & Smolich, 2015; Charlton *et al.*, 2019), although Reymond *et al.* (2009) later developed a similar empirical relationship based on published in vivo wave speeds. The drawback of these empirical relationships is that they provide similar wave speeds for arteries of similar radius but different wall properties (e.g., common carotid and femoral arteries). We have shown that our improved relationship provides substantially more accurate estimates of wave speed across a wide range of central and peripheral arteries in the young adult compared to previously employed relationships because it accounts for different wall properties as well as radius.

We incorporated impedance-preserving taper in the YoungAdult model, which moved the major reflection sites distally to the vascular beds. Many previous studies have incorporated substantial within-segment taper (of up to 70% by area (Mynard & Smolich, 2015)) into cardiovascular models (Stergiopulos *et al.*, 1992; Reymond *et al.*, 2009). Although arterial diameter is known to decrease with distance from the heart, Suwa *et al.* (1963) and Milnor and Bertram (1978) found little to no taper in sections of arteries between successive branching points. This led Papageorgiou and Jones (1987) to conclude that the reduction in diameter of an artery does not occur continuously (as assumed in previous models), but in steps, with each step occurring due to branching of the vascular tree. Implementing such impedance-preserving tapering in the YoungAdult model led to substantial changes in both central and peripheral arteries, compared with the Mynard2015 model (Mynard & Smolich, 2015), i.e. leading to an ascending aortic pressure waveform exhibiting the typical features of a young adult, as well as triphasic flow in peripheral arteries.

Additional evidence towards the lack of within-segment taper arises when considering model findings in Figure 8 in light of experimental data presented by van den Bos *et al.* (1982). These authors found that substantial reduction of peripheral resistance and vascular bed wave reflection, via administration of the potent vasodilator sodium

nitroprusside in dogs, led to pressure and flow waveforms in the ascending aorta having similar shapes. This indicated that vascular beds are likely to be the main sites of wave reflection. Our results are consistent with this conclusion, since increasing C_{bed} in the YoungAdult model produced similar pressure and flow waveforms in the ascending aorta (Figure 8d) as in van den Bos *et al.* (1982), noting that C_{bed} is likely to increase with vasodilation. By contrast, even with a large increase in C_{bed} in the Mynard2015 model (that includes substantial within-segment taper), the ascending aortic pressure and flow waveforms still had dissimilar shapes, indicating that significant arterial wave reflection was still present within the 1D network (i.e. conduit arteries).

Our findings therefore support the contention by Papageorgiou and Jones (1987) that 'true' arterial taper (i.e. within-segment taper) is unlikely to be a typical (or at least haemodynamically significant) feature in healthy young adults, and that vascular beds are the main sites of wave reflection in the vasculature (O'Rourke & Kelly, 1993). Indeed, from a design point of view, it is unclear why such within-segment taper would be beneficial. It was therefore not surprising that eliminating this impedance-increasing taper from the major arteries in the YoungAdult model caused wave reflection to occur more distally in the network, and the reflected waves to arrive in the ascending aorta during diastole. The reflected waves thus exerted minimal effect during systole (resulting in an early systolic peak and negative augmentation) but a prominent influence during diastole (resulting in the diastolic hump), which is an optimal situation when considering cardiac energetics (O'Rourke & Hashimoto, 2007).

The influence of C_{bed} in 1D models has received little attention, but we observed this parameter has a substantial effect on wave reflection properties in the vasculature. Importantly, we showed that the 'subtraction approach' to approximate C_{bed}, may not provide accurate values since calculated total arterial compliance (using model waveforms) is relatively insensitive to this quantity (Supplemental File 1 – Part C). Hence, we explored the effect of varying C_{bed} on flow waveforms of distal arteries. Reflection from systemic vascular beds would produce a backward compression wave (BCW) on wave intensity analysis (Parker, 2009; Mynard *et al.*, 2020), the amplitude of which would be inversely related to C_{bed} (given that reducing C_{bed} increases reflection). The BCW would decrease arterial flow (Parker, 2009), tending to produce backward flow and the triphasic flow patterns seen under healthy conditions (Rangankar *et al.*, 2016). This explains why decreasing C_{bed} (increased wave reflection) increased the triphasic nature of flow and caused earlier diastolic flow reversal but increasing C_{bed} (reduced wave reflection) decreased it and made it more monophasic in nature. In fact, a monophasic flow waveform in distal arteries can point to a pathological condition such as stenosis (Stergiopulos *et al.*, 1992; Donnelly *et al.*, 2000; Rangankar *et al.*, 2016). Previous models have produced monophasic femoral flow waveforms (Stergiopulos *et al.*, 1992; Reymond *et al.*, 2009), suggesting that the C_{bed} values and/or vascular geometry may have been underestimated. Given that the precise value of C_{bed} is not currently known, our results suggest that the dominant effect of C_{bed} on the triphasic flow of distal arteries may be useful in guiding estimation of C_{bed}.

It is of interest that reducing C_{bed} had a similar effect on both the pressure and flow waveforms: increased early systolic peak, lower early diastolic trough, and increased late systolic hump. This may be counterintuitive because a BCW has opposite effects on pressure and flow (Parker, 2009; Mynard *et al.*, 2020). However, the similar effects of C_{bed} observed in conduit arteries likely relates to the fact that at arterial bifurcations, reflected waves from a given branch are transmitted into all other branches (not just the parent artery) (Mynard *et al.*, 2017); therefore, they give rise to backward waves as well as forward waves in peripheral arteries. Although the complex ensemble of reflected, re-reflected, and transmitted waves makes it difficult to precisely establish the basis for all waveform features, changes in pressure and flow that are in the same direction indicate a predominant effect of forward waves whereas changes in the opposite direction indicate a predominant effect of backward waves.

While it is known that the diastolic hump in the ascending aortic pressure waveform is caused by the reflected waves arriving during diastole (O'Rourke & Yaginuma, 1984),

the exact origin of these reflected waves is unclear. Based on in vivo experiments, O'Rourke and Taylor (1967) proposed that there were two distinct 'effective' reflection sites in the body roughly corresponding to the upper and lower body. They consequently likened the systemic arterial network to an asymmetric T-Tube model, with the shorter tube representing the upper body and the longer tube representing the lower body (O'Rourke, 1967). They also proposed that, in young adults, reflections from the upper body and lower body affect the early and later part of the cardiac cycle, respectively (O'Rourke & Avolio, 1980). Our simulations were consistent with this concept given that increasing reflection from the arm/cerebral and leg arteries increased the late systolic portion and diastolic hump of the ascending aortic pressure waveform, respectively, thus providing insight into the effect of wave reflection from different regions of the body on the ascending aortic pressure waveform.

Given the clear influence of wave reflection from the legs on the diastolic hump (see Figure 5), it was not surprising that this waveform feature was affected by the reflection properties of the aortoiliac bifurcation. While most arterial junctions appear to be well matched in the forward direction, the aortoiliac bifurcation is thought to be a potential exception due to observed lower daughter-to-parent area ratios (Papageorgiou *et al.*, 1990). Ex vivo analysis of abdominal aortic and common iliac arteries by Greenwald et al. suggested that R_p at the aortoiliac bifurcation might reach 0.2 or even higher in some young individuals, although most values in young adults were between 0 and 0.1 (Greenwald *et al.*, 1990). Our results show that introducing $R_p = 0.2$ at the aortoiliac bifurcation abolished the diastolic hump, indicating that the earlier wave reflection arriving at the aorta due to the unmatched junction obscures the impact of reflection in the legs (as revealed by comparison with $R_p = 0$ (Figures 5 and 7). These findings suggest that the aortoiliac bifurcation (in addition to other arterial junctions in the lower body) may need to be well-matched to obtain a prominent diastolic hump, although this needs to be investigated in future human studies.

There are some limitations that should be considered when interpreting the results of this study. First, for simplicity and consistency, a single value of $\tau = 1.3$ was used for all vascular beds. Although this produced acceptable waveforms in all arteries, we did observe that using $\tau = 0.5$ in just the arm vascular beds (with $\tau = 1.3$ in all other beds) produced arm waveforms that were closer to those obtained in vivo compared to the baseline model (Figure 4); however, using $\tau = 0.5$ in all vascular beds abolished the early systolic peak and negative augmentation in the ascending aortic pressure waveform. Thus, future studies could investigate methods for estimating C_{bed} of individual vascular beds more precisely. Second, directly obtaining the ascending aortic pressure waveform was beyond the scope of the study; hence, it had to be estimated using a transfer function applied to the carotid pressure waveform, which could potentially reduce the accuracy of the in vivo systolic and pulse pressure values obtained for the ascending aorta. Although the resulting ascending aortic pulse pressure was lower than that calculated in our cohort, the value obtained was within the normal range compared to literature data (McEniery *et al.*, 2005).

In conclusion, we have shown that the YoungAdult systemic arterial network model incorporating more accurate arterial wave speeds, impedance-preserving taper and well-matched junctions exhibits reflected waves that predominantly arise at the level of the vascular beds and arrive in the ascending aorta during the diastolic period. These physiological features produce waveform features that are typical of a healthy young adult, including an early systolic peak, negative augmentation, and a diastolic hump in the ascending aorta, as well as triphasic flow in peripheral arteries. Our model provides novel insights into the 'fine-tuning' of arterial network properties, and it can be used as a baseline in future studies of cardiovascular ageing and disease.

Author Contributions: A.K. and J.P.M. contributed to the conception and design of the work. A.K., H.A.H, J.J.S., M.M.H.C, and J.P.M. contributed to the acquisition, analysis, or interpretation of data

for the work. A.K., H.A.H, J.J.S., M.M.H.C., and J.P.M. contributed to drafting and revising the manuscript.

All authors:

i. approve the final version of the manuscript.

ii. agree to be accountable for all aspects of the work.

iii. declare that all persons designated as authors qualify for authorship, and all those who qualify for authorship are listed.

Funding: J.P.M. was supported by a co-funded Career Development Fellowship from the National Health and Medical Research Council of Australia (APP1143510) and Future Leader Fellowship from the National Heart Foundation of Australia (101199). The Heart Research group at the Murdoch Children's Research Institute is supported by the Victorian Government's Operational Infrastructure Program, RCH 1000 and Big W.

Data Availability Statement: The raw data from the YoungAdult model will be made available upon reasonable request.

Conflicts of Interest: The authors declare no conflict of interest.

References

1. Alastruey J, Parker K, Peiró J & Sherwin S. (2009). Analysing the pattern of pulse waves in arterial networks: A time-domain study. *J Eng Math* **64,** 331-351.
2. Avolio A. (1980a). Multi-branched model of the human arterial system. *Med Biol Eng Comput* **18,** 709-718.
3. Avolio AP. (1980b). Multi-branched model of the human arterial system. *Med Biol Eng Comput* **18,** 709-718.
4. Beniwal S, Bhargava K & Kausik SK. (2014). Size of distal radial and distal ulnar arteries in adults of southern rajasthan and their implications for percutaneous coronary interventions. *Indian Heart J* **66,** 506-509.
5. Betts JG, Desaix P, Johnson E, Johnson JE, Korol O, Kruse D, Poe B, Wise JA, Womble M & Young KA. (2013). *Anatomy & physiology*. OpenStax College, Rice University.
6. Bjarnegård N & Länne T. (2010). Arterial properties along the upper arm in humans: Age-related effects and the consequence of anatomical location. *J Appl Physiol (1985)* **108,** 34-38.
7. Black CD, Vickerson B & McCully KK. (2003). Noninvasive assessment of vascular function in the posterior tibial artery of healthy humans. *Dyn Med* **2,** 1.
8. Blanco P, Watanabe S, Passos M, Lemos P & Feijoo R. (2014). An anatomically detailed arterial network model for one-dimensional computational hemodynamics. *IEEE Trans Biomed Eng* **62,** 736-753.
9. Bossuyt J, Engelen L, Ferreira I, Stehouwer CD, Boutouyrie P, Laurent S, Segers P, Reesink K, Van Bortel LM & Collaboration obotRVfAM. (2015). Reference values for local arterial stiffness. Part b: Femoral artery. *J Hypertens* **33,** 1997-2009.
10. Brandfonbrener M, Landowne M & Shock NW. (1955). Changes in cardiac output with age. *Circulation* **12,** 557-566.
11. Charlton PH, Mariscal Harana J, Vennin S, Li Y, Chowienczyk P & Alastruey J. (2019). Modeling arterial pulse waves in healthy aging: A database for in silico evaluation of hemodynamics and pulse wave indexes. *Am J Physiol Heart Circ Physiol* **317,** H1062-h1085.
12. Chen C-H, Ting C-T, Nussbacher A, Nevo E, Kass DA, Pak P, Wang S-P, Chang M-S & Yin FCP. (1996). Validation of carotid artery tonometry as a means of estimating augmentation index of ascending aortic pressure. *Hypertension* **27,** 168-175.
13. Chirinos JA, Kips JG, Jacobs DR, Brumback L, Duprez DA, Kronmal R, Bluemke DA, Townsend RR, Vermeersch S & Segers P. (2012a). Arterial wave reflections and incident cardiovascular events and heart failure: Mesa (multiethnic study of atherosclerosis). *J Am Coll Cardiol* **60,** 2170-2177.
14. Chirinos JA, Segers P, Gillebert TC, Gupta AK, De Buyzere ML, De Bacquer D, St John-Sutton M & Rietzschel ER. (2012b). Arterial properties as determinants of time-varying myocardial stress in humans. *Hypertension* **60,** 64-70.
15. De Hoon J, Willigers J, Troost J, Struijker-Boudier H & Van Bortel L. (2003). Cranial and peripheral interictal vascular changes in migraine patients. *Cephalalgia* **23,** 96-104.
16. Donnelly R, Hinwood D & London NJ. (2000). Abc of arterial and venous disease. Non-invasive methods of arterial and venous assessment. *BMJ* **320,** 698-701.
17. Engelen L, Bossuyt J, Ferreira I, van Bortel LM, Reesink KD, Segers P, Stehouwer CD, Laurent S & Boutouyrie P. (2015). Reference values for local arterial stiffness. Part a: Carotid artery. *J Hypertens* **33,** 1981-1996.
18. Gerhard-Herman M, Gardin JM, Jaff M, Mohler E, Roman M & Naqvi TZ. (2006). Guidelines for noninvasive vascular laboratory testing: A report from the american society of echocardiography and the society for vascular medicine and biology. *Vasc Med* **11,** 183-200.
19. Greenwald SE, Carter AC & Berry CL. (1990). Effect of age on the in vitro reflection coefficient of the aortoiliac bifurcation in humans. *Circulation* **82,** 114-123.
20. Groenink M, de Roos A, Mulder BJ, Spaan JA & van der Wall EE. (1998). Changes in aortic distensibility and pulse wave velocity assessed with magnetic resonance imaging following beta-blocker therapy in the marfan syndrome. *Am J Cardiol* **82,** 203-208.

21. Hamilton WF. (1944). The patterns of the arterial pressure pulse. *Am J Physiol* **141,** 235-241.
22. Hansen KW & Orskov H. (1992). A plea for consistent reliability in ambulatory blood pressure monitors: A reminder. *J Hypertens* **10,** 1313-1315.
23. Hwang JY. (2017). Doppler ultrasonography of the lower extremity arteries: Anatomy and scanning guidelines. *Ultrasonography* **36,** 111-119.
24. Jourdan C, Wühl E, Litwin M, Fahr K, Trelewicz J, Jobs K, Schenk JP, Grenda R, Mehls O, Tröger J & Schaefer F. (2005). Normative values for intima-media thickness and distensibility of large arteries in healthy adolescents. *J Hypertens* **23,** 1707-1715.
25. Katori R. (1979). Normal cardiac output in relation to age and body size. *Tohoku J Exp Med* **128,** 377-387.
26. Kelly R & Fitchett D. (1992). Noninvasive determination of aortic input impedance and external left ventricular power output: A validation and repeatability study of a new technique. *J Am Coll Cardiol* **20,** 952-963.
27. Kelly R, Hayward C, Avolio A & O'Rourke M. (1989). Noninvasive determination of age-related changes in the human arterial pulse. *Circulation* **80,** 1652-1659.
28. Kim EK, Chang SA, Jang SY, Kim Y, Kim SM, Oh JK, Choe YH & Kim DK. (2013). Assessment of regional aortic stiffness with cardiac magnetic resonance imaging in a healthy asian population. *Int J Cardiovasc Imaging* **29 Suppl 1,** 57-64.
29. Kim ES, Sharma AM, Scissons R, Dawson D, Eberhardt RT, Gerhard-Herman M, Hughes JP, Knight S, Marie Kupinski A, Mahe G, Neumyer M, Poe P, Shugart R, Wennberg P, Williams DM & Zierler RE. (2020). Interpretation of peripheral arterial and venous doppler waveforms: A consensus statement from the society for vascular medicine and society for vascular ultrasound. *Vasc Med* **25,** 484-506.
30. Kondiboyina A, Smolich JJ, Cheung MMH, Westerhof BE & Mynard JP. (2020). Conduit arterial wave reflection promotes pressure transmission but impedes hydraulic energy transmission to the microvasculature. *Am J Physiol Heart Circ Physiol* **319,** H66-H75.
31. Latham RD, Westerhof N, Sipkema P, Rubal BJ, Reuderink P & Murgo JP. (1985). Regional wave travel and reflections along the human aorta: A study with six simultaneous micromanometric pressures. *Circulation* **72,** 1257-1269.
32. Learoyd BM & Taylor MG. (1966). Alterations with age in the viscoelastic properties of human arterial walls. *Circ Res* **18,** 278-292.
33. Lee HY & Oh BH. (2010). Aging and arterial stiffness. *Circ J* **74,** 2257-2262.
34. Leloup AJ, Van Hove CE, Heykers A, Schrijvers DM, De Meyer GR & Fransen P. (2015). Elastic and muscular arteries differ in structure, basal no production and voltage-gated ca(2+)-channels. *Front Physiol* **6,** 375.
35. Lockwood GR, Ryan LK, Gotlieb AI, Lonn E, Hunt JW, Liu P & Foster FS. (1992). In vitro high resolution intravascular imaging in muscular and elastic arteries. *J Am Coll Cardiol* **20,** 153-160.
36. Lorbeer R, Grotz A, Dörr M, Völzke H, Lieb W, Kühn JP & Mensel B. (2018). Reference values of vessel diameters, stenosis prevalence, and arterial variations of the lower limb arteries in a male population sample using contrast-enhanced mr angiography. *PLoS One* **13,** e0197559.
37. Maixner W, Wright CB, Schoepfle WJ & Barnes RW. (1980). Femoral artery flow velocities: A sensitive index of limb hemodynamics associated with venous occlusion. *J Surg Res* **29,** 326-330.
38. Master AM, Dublin LI & Marks HH. (1950). The normal blood pressure range and its clinical implications. *J Am Med Assoc* **143,** 1464-1470.
39. McEniery CM, Yasmin, Hall IR, Qasem A, Wilkinson IB & Cockcroft JR. (2005). Normal vascular aging: Differential effects on wave reflection and aortic pulse wave velocity: The anglo-cardiff collaborative trial (acct). *J Am Coll Cardiol* **46,** 1753-1760.
40. Mikola H, Pahkala K, Rönnemaa T, Viikari JSA, Niinikoski H, Jokinen E, Salo P, Simell O, Juonala M & Raitakari OT. (2015). Distensibility of the aorta and carotid artery and left ventricular mass from childhood to early adulthood. *Hypertension* **65,** 146-152.
41. Milnor WR & Bertram CD. (1978). The relation between arterial viscoelasticity and wave propagation in the canine femoral artery in vivo. *Circ Res* **43,** 870-879.
42. Murgo JP, Westerhof N, Giolma JP & Altobelli SA. (1980). Aortic input impedance in normal man: Relationship to pressure wave forms. *Circulation* **62,** 105-116.
43. Mynard JP, Kondiboyina A, Kowalski R, Cheung MMH & Smolich JJ. (2020). Measurement, analysis and interpretation of pressure/flow waves in blood vessels. *Front Physiol* **11**.
44. Mynard JP, Kowalski R, Cheung MMH & Smolich JJ. (2017). Beyond the aorta: Partial transmission of reflected waves from aortic coarctation into supra-aortic branches modulates cerebral hemodynamics and left ventricular load. *Biomech Model Mechanobiol* **16,** 635-650.
45. Mynard JP & Nithiarasu P. (2008). A 1d arterial blood flow model incorporating ventricular pressure, aortic valve and regional coronary flow using the locally conservative galerkin (lcg) method. *Comm Num Meth Eng* **24,** 367-417.
46. Mynard JP & Smolich JJ. (2015). One-dimensional haemodynamic modeling and wave dynamics in the entire adult circulation. *Ann Biomed Eng* **43,** 1443-1460.
47. Negoita M, Hughes AD, Parker KH & Khir AW. (2018). A method for determining local pulse wave velocity in human ascending aorta from sequential ultrasound measurements of diameter and velocity. *Physiol Meas* **39,** 114009.
48. Nichols WW. (1998). *Mcdonald's blood flow in arteries: Theoretical, experimental, and clinical principles / wilmer w. Nichols, michael f. O'rourke ; with a contribution from craig hartley*. Arnold ; Oxford University Press, London : New York.
49. Nichols WW, O'Rourke MF, Avolio AP, Yaginuma T, Murgo JP, Pepine CJ & Conti CR. (1985). Effects of age on ventricular-vascular coupling. *Am J Cardiol* **55,** 1179-1184.

50. Noordergraaf A, Verdouw PD & Boom HBK. (1963). The use of an analog computer in a circulation model. *Prog Cardiovasc Dis* **5,** 419-439.
51. Nowrozani FR & Zareiyan B. (2011). A microscopic study of the external carotid artery transitional zone of the adult male dog. *J Appl Anim Res* **39,** 406-411.
52. O'Rourke MF. (1967). Pressure and flow waves in systemic arteries and the anatomical design of the arterial system. *J Appl Physiol* **23,** 139-149.
53. O'Rourke MF. (1982). *Arterial function in health and disease*. Churchill Livingstone.
54. O'Rourke MF. (1984). Wave reflections and the arterial pulse. *Arch Intern Med* **144,** 366.
55. O'Rourke MF & Avolio AP. (1980). Pulsatile flow and pressure in human systemic arteries. Studies in man and in a multi-branched model of the human systemic arterial tree. *Circ Res* **46,** 363-372.
56. O'Rourke MF & Hashimoto J. (2007). Mechanical factors in arterial aging: A clinical perspective. *J Am Coll Cardiol* **50,** 1-13.
57. O'Rourke MF & Kelly RP. (1993). Wave reflection in the systemic circulation and its implications in ventricular function. *J Hypertens* **11,** 327-337.
58. O'Rourke MF & Nichols WW. (2005). Aortic diameter, aortic stiffness, and wave reflection increase with age and isolated systolic hypertension. *Hypertension* **45,** 652-658.
59. O'Rourke MF & Taylor MG. (1967). Input impedance of the systemic circulation. *Circ Res* **20,** 365-380.
60. O'Rourke MF & Yaginuma T. (1984). Wave reflections and the arterial pulse. *Arch Intern Med* **144,** 366-371.
61. Olufsen MS. (1999). Structured tree outflow condition for blood flow in larger systemic arteries. *Am J Physiol Heart Circ Physiol* **276,** H257-H268.
62. Papageorgiou GL, Jones BN, Redding VJ & Hudson N. (1990). The area ratio of normal arterial junctions and its implications in pulse wave reflections. *Cardiovasc Res* **24,** 478-484.
63. Papageorgiou GL & Jones NB. (1987). Arterial system configuration and wave reflection. *J Biomed Eng* **9,** 299-301.
64. Parker KH. (2009). An introduction to wave intensity analysis. *Med Biol Eng Comput* **47,** 175.
65. Petersen SE, Wiesmann F, Hudsmith LE, Robson MD, Francis JM, Selvanayagam JB, Neubauer S & Channon KM. (2006). Functional and structural vascular remodeling in elite rowers assessed by cardiovascular magnetic resonance. *J Am Coll Cardiol* **48,** 790-797.
66. Phan TS, Li JKJ, Segers P & Chirinos JA. (2016). Misinterpretation of the determinants of elevated forward wave amplitude inflates the role of the proximal aorta. *J Am Heart Assoc* **5,** e003069.
67. Pomella N, Wilhelm EN, Kolyva C, Gonzalez-Alonso J, Rakobowchuk M & Khir AW. (2017). Common carotid artery diameter, blood flow velocity and wave intensity responses at rest and during exercise in young healthy humans: A reproducibility study. *Ultrasound Med Biol* **43,** 943-957.
68. Rakobowchuk M, Stuckey MI, Millar PJ, Gurr L & Macdonald MJ. (2009). Effect of acute sprint interval exercise on central and peripheral artery distensibility in young healthy males. *Eur J Appl Physiol* **105,** 787-795.
69. Rakobowchuk M, Tanguay S, Burgomaster KA, Howarth KR, Gibala MJ & MacDonald MJ. (2008). Sprint interval and traditional endurance training induce similar improvements in peripheral arterial stiffness and flow-mediated dilation in healthy humans. *Am J Physiol Regul Integr Comp Physiol* **295,** R236-242.
70. Rangankar VP, Taori KB, Mundhada RG & Rewatkar AD. (2016). Accuracy of common femoral artery doppler waveform analysis in predicting haemodynamically significant aortoiliac lesions. *J Clin Diagn Res* **10,** Tc26-28.
71. Rees PM. (1968). Electron microscopical observations on the architecture of the carotid arterial walls, with special reference to the sinus portion. *J Anat* **103,** 35-47.
72. Reymond P, Merenda F, Perren F, Rüfenacht D & Stergiopulos N. (2009). Validation of a one-dimensional model of the systemic arterial tree. *Am J Physiol Heart Circ Physiol* **297,** H208-H222.
73. Reymond P, Westerhof N & Stergiopulos N. (2012). Systolic hypertension mechanisms: Effect of global and local proximal aorta stiffening on pulse pressure. *Ann Biomed Eng* **40,** 742-749.
74. Rittenhouse EA, Maxiner W, Burr JW & Barnes RW. (1976). Directional arterial flow velocity: A sensitive index of changes in peripheral vascular resistance. *Surgery* **79,** 350-355.
75. Robinson SC & Brucer M. (1939). Range of normal blood pressure: A statistical and clinical study of 11,383 persons. *Arch Intern Med* **64,** 409-444.
76. Rogers WJ, Hu Y-L, Coast D, Vido DA, Kramer CM, Pyeritz RE & Reichek N. (2001). Age-associated changes in regional aortic pulse wave velocity. *J Am Coll Cardiol* **38,** 1123-1129.
77. Sabatier MJ, Stoner L, Reifenberger M & McCully K. (2006). Doppler ultrasound assessment of posterior tibial artery size in humans. *J Clin Ultrasound* **34,** 223-230.
78. Segers P & Verdonck P. (2000). Role of tapering in aortic wave reflection: Hydraulic and mathematical model study. *J Biomech* **33,** 299-306.
79. Sherwin SJ, Franke V, Peiró J & Parker K. (2003). One-dimensional modelling of a vascular network in space-time variables. *J Eng Math* **47,** 217-250.
80. Sluyter JD, Hughes AD, Camargo CA, Thom SAM, Parker KH, Hametner B, Wassertheurer S & Scragg R. (2019). Identification of distinct arterial waveform clusters and a longitudinal evaluation of their clinical usefulness. *Hypertension* **74,** 921-928.
81. Stergiopulos N, Meister JJ & Westerhof N. (1994). Simple and accurate way for estimating total and segmental arterial compliance: The pulse pressure method. *Ann Biomed Eng* **22,** 392-397.

82. Stergiopulos N, Young DF & Rogge TR. (1992). Computer simulation of arterial flow with applications to arterial and aortic stenoses. *J Biomech* **25,** 1477-1488.
83. Suwa N, Niwa T, Fukasawa H & Sasaki Y. (1963). Estimation of intravascular blood pressure gradient by mathematical analysis of arterial casts. *Tohoku J Exp Med* **79,** 168-198.
84. Tomiyama H, Komatsu S, Shiina K, Matsumoto C, Kimura K, Fujii M, Takahashi L, Chikamori T & Yamashina A. (2018). Effect of wave reflection and arterial stiffness on the risk of development of hypertension in japanese men. *J Am Heart Assoc* **7,** e008175.
85. van den Berkmortel F, Wollersheim H, van Langen H & Thien T. (1998). Dynamic vessel wall properties and their reproducibility in subjects with increased cardiovascular risk. *J Hum Hypertens* **12,** 345-350.
86. van den Bos GC, Westerhof N & Randall OS. (1982). Pulse wave reflection: Can it explain the differences between systemic and pulmonary pressure and flow waves? A study in dogs. *Circ Res* **51,** 479-485.
87. Vennin S, Li Y, Mariscal Harana J, Charlton P, Fok H, Gu H, Chowienczyk P & Alastruey J. (2021). Novel pressure wave separation analysis for cardiovascular function assessment highlights major role of aortic root. *IEEE Trans Biomed Eng* **Pp**.
88. Westerhof BE, van den Wijngaard JP, Murgo JP & Westerhof N. (2008). Location of a reflection site is elusive: Consequences for the calculation of aortic pulse wave velocity. *Hypertension* **52,** 478-483.
89. Westerhof BE & Westerhof N. (2018). Uniform tube models with single reflection site do not explain aortic wave travel and pressure wave shape. *Physiol Meas* **39,** 124006.
90. Westerhof N, Bosman F, De Vries CJ & Noordergraaf A. (1969a). Analog studies of the human systemic arterial tree. *J Biomech* **2,** 121-134.
91. Westerhof N, Bosman F, De Vries CJ & Noordergraaf A. (1969b). Analog studies of the human systemic arterial tree. *J Biomech* **2,** 121-143.
92. Westerhof N, Sipkema P, van den Bos GC & Elzinga G. (1972). Forward and backward waves in the arterial system. *Cardiovasc Res* **6,** 648-656.
93. Yoo B-S, Lee S-H, Ko J-Y, Lee B-K, Kim S-N, Lee M-O, Hwang S-O, Choe K-H & Yoon J. (2003). Procedural outcomes of repeated transradial coronary procedure. *Catheter Cardiovasc Interv* **58,** 301-304.
94. Yoo B-S, Yoon J, Ko J-Y, Kim J-Y, Lee S-H, Hwang S-O & Choe K-H. (2005). Anatomical consideration of the radial artery for transradial coronary procedures: Arterial diameter, branching anomaly and vessel tortuosity. *Int J Cardiol* **101,** 421-427.
95. Zhou Z, Xing A-J, Zhang J-N, Xia W-H, Su C, Xu S-Y, Zhang X-Y, Chen S-H, Huang Z, Qian X-X, Wu S-L & Tao J. (2021). Hypertension, arterial stiffness, and clinical outcomes: A cohort study of chinese community-based population. *Hypertension* **78,** 333-341.